



Analysis of the Microstructure Role in the Yield Asymmetry of Extruded Mg-LPSO Alloys Using In Situ Diffraction Experiments

G. GARCES,¹ J. MEDINA,¹ P. PEREZ,¹ A. STARK,² H.K. LIM,³
S. KIM,³ N. SHELL,⁴ and P. ADEVA^{1,5} 

1.—Department of Physical Metallurgy, CENIM-CSIC, Avenida Gregorio del Amo 8, 28040 Madrid, Spain. 2.—Institute of Materials Research, Helmholtz-Zentrum Geesthacht, Max-Planck-Str. 1, 21502 Geesthacht, Germany. 3.—Korea Institute of Industrial Technology (KITECH), 156 Gaetbeol-ro, Yeonsu-gu, Incheon 21999, Korea. 4.—Structural Research on New Materials, Helmholtz-Zentrum Geesthacht Outstation at DESY, Notkestraße 85, 22607 Hamburg, Germany. 5.—e-mail: adeva@cenim.csic.es

The effect of microstructure and processing parameters on the mechanical behavior of extruded Mg-Y_{2x}-Zn_x alloys containing different volume fractions of the long-period stacking order (LPSO) phase is evaluated using in situ diffraction experiments. The Mg-LPSO extruded alloys exhibit a microstructure consisting of a mixture of fine dynamically recrystallized α -Mg grains, highly oriented non-recrystallized coarse α -Mg grains with the basal plane parallel to the extrusion direction, and particles of the LPSO phase elongated in the extrusion direction. The volume fraction of dynamically recrystallized α -Mg grain areas tends to increase as the volume fraction of the LPSO phase and the processing stress increase. In situ diffraction experiments have allowed the understanding of the elastic–plastic behavior of non-DRXed and DRXed grains, and their individual contribution to the macroscopic deformation of magnesium alloys containing LPSO phases and, consequently, the reverse tension–compression asymmetry.

INTRODUCTION

Mg-Y_{2x}-Zn_x alloys contain a long-period stacking ordered (LPSO) phase. This phase provides the alloy with mechanical properties superior to those of commercial magnesium alloys, which makes them very competitive for multiple applications, especially in the automotive, aeronautical, and electronic industries. The LPSO phase, independently of its crystal structure (18R, 16H, 10H), shows stacking and chemical ordering along the basal plane.^{1–5}

The as-cast Mg-LPSO alloys have a two-phase microstructure consisting of Mg dendrites in which the LPSO phase is located at inter-dendritic spaces. After extrusion, the alloy acquires an intense crystallographic texture. The LPSO phase elongates in

the extrusion direction, while the Mg matrix is composed of areas with fine dynamically recrystallized (DRXed) α -Mg grains and areas consisting of very coarse non-recrystallized (non-DRXed) α -Mg grains. The latter are sharply textured with their basal plane parallel to the extrusion direction.^{6–8} The hexagonal close-packed lattice of Mg, with a limited number of active deformation systems, promotes the formation of a strong crystallographic texture when the alloy is thermomechanically processed, inducing the tension–compression yield asymmetry phenomenon. The mechanical asymmetry of Mg alloys has been widely investigated, since is an important factor limiting their applications.^{9–13}

In the case of extruded Mg alloys, this is reflected by higher yield strength values under tensile loads applied in the extrusion direction compared with those under compressive loads. However, {10 $\bar{1}$ 2} tensile twinning can be active under compression

along the extrusion direction, resulting in a decrease in the compressive yield stress with respect to the tensile yield stress.¹⁴

Different asymmetric yield behavior is observed, however, in the case of Mg alloys with random texture. Activation of the {10–12} twinning system, which governs the initial stages of deformation, is notably different under tension and compression, resulting in a lower yield strength value and higher strain-hardening under tension than under compression.¹⁵

Yield anisotropy is still more complicated in Mg-Y-Zn alloys containing the LPSO phase. This phase has a coherent (0001) basal plane with a Mg matrix, while their stacking sequence is modified along the *c*-axis compared to that of Mg. The effect of LPSO phase on yield asymmetry has been studied in as-cast alloys. The alloy tensile tested showed low ductility, observing that the LPSO phase fractured. A study of samples after compression tests showed kink bands in the LPSO phase, which form by the cooperative initiation and/or synchronized slip, and even rearrangement of basal dislocations. The kink bands can cause refinement of large LPSO phase particles, and transplant them into adjacent Mg grains to form kink boundaries. Both, kink bands and kink boundaries seem to be very effective in refining the microstructure and improving the strength of the alloy, resulting in a relatively high compressive yield strength and evident yield asymmetry.¹⁶

Furthermore, it can be expected that microstructural constituents in an extruded Mg-LPSO alloy have a different elastic–plastic behavior, while its mechanical behavior will strongly depend strongly on the volume fraction and texture of each of them. For instance, the tension–compression asymmetry in wrought Mg alloys, characterized by a tensile yield stress higher than the compressive yield stress when the load is applied in the extrusion direction, is reversed when the volume fraction of the LPSO phase is higher than 10%,¹⁷ attaining yield strength values higher in compression than in tension. Using synchrotron diffraction during in situ mechanical tests, it has been proved that the beginning of the plasticity (yield stress) under compression in an Mg-Y-Zn alloy, with a LPSO volume fraction of

approximately 20 %, is related to the activation of the basal slip system in DRXed grains which are randomly oriented.¹⁸ However, highly oriented non-DRXed grains yield at lower stresses than randomly oriented DRXed grains, due to the activation of tensile twinning in these grains.¹⁴

Since the volume fraction of DRXed grains is much higher compared to non-DRXed grains, the macroscopic yielding is controlled by ultrafine equiaxed grains.¹⁹

Consequently, it can be expected that tension–compression asymmetry will follow the “normal” behavior of extruded magnesium alloys, regardless of the volume fraction of the LPSO phase, on the assumption that the volume fraction of non-DRXed grains was higher than that of DRXed grains.

This article is focused on elucidating this hypothesis in Mg-Y_{2x}-Zn_x alloys. For this purpose, alloys with different Y and Zn contents have been prepared and extruded with different extrusion ratios, in order to obtain materials with different volume fractions of the aforementioned microstructural constituents. In situ synchrotron diffraction experiments during tensile and compression tests were conducted to identify the type of α -Mg grains (DRXed or non-DRXed), and the deformation mechanism (dislocation slip or tensile twinning) macroscopically controlling the beginning of the plastic deformation.

EXPERIMENTAL PROCEDURE

Three alloys, designated as Mg₉₇Y₁Zn_{0.5}, Mg₉₇Y₂Zn₁, and Mg₉₇Y₃Zn_{1.5}, were obtained by melting and casting using an electric resistance furnace. The composition of the alloys, determined by wavelength-dispersive x-ray spectroscopy, are given in wt.% in Table I.

Billets were extruded at 350°C at an extrusion speed of 0.5 mms⁻¹, with reduction ratios of 18:1, 10:1, and 4:1, and, therefore, the extrusion strains, ϵ_T , were 2.9, 2.3, and 1.4, respectively.

The microstructure of the alloys was studied by scanning electron microscopy. The samples were prepared by mechanical polishing and etching with a solution of 5 ml of acetic acid, 20 ml of water, and 25 ml of picric acid in methanol. Grain size and

Table I. Designation and composition in wt.% of the three alloys, and volume fractions of the LPSO phase, recrystallized areas (DRXed), and non-recrystallized areas (non-DRXed) for each alloy composition in the three extrusion strains

Designation	Composition wt.%	Vf (%) LPSO	DRXed areas, Vf (%)			Non-DRXed areas, Vf (%)		
			$\epsilon_T = 1.4$	$\epsilon_T = 2.3$	$\epsilon_T = 2.9$	$\epsilon_T = 1.4$	$\epsilon_T = 2.3$	$\epsilon_T = 2.9$
MgY ₁ Zn _{0.5}	Mg-3.6Y-1.6Zn	7	35	45	46	58	48	47
MgY ₂ Zn ₁	Mg-6.9Y-2.5Zn	19	38	51	57	43	30	24
MgY ₃ Zn _{1.5}	Mg-10Y-3.7Zn	32	28	57	60	40	11	8

volume fraction of the DRXed and non-DRXed areas were measured by quantitative image analysis using Sigma Scan Pro software.

The crystallographic texture of the extruded alloys was determined by means of x-ray diffraction, using a Siemens TM Kristalloflex D5000 diffractometer with β -filtered Cu-K α radiation. The orientation distribution function was computed from the experimental $\{10\bar{1}0\}$, $\{0002\}$, $\{10\bar{1}1\}$, $\{10\bar{1}2\}$, $\{10\bar{1}3\}$, and $\{11\bar{2}0\}$ pole figures by the series expansion method, considering the z -axis to be parallel to the extrusion direction.

Synchrotron radiation diffraction was carried out during in situ tension and compression tests at the P07-HEMS beamline of PETRA III, at the Deutsches Elektronen-Synchrotron. Samples for the compression tests were cylinders of 5 mm in diameter and 10 mm in length machined along the extrusion direction. Samples for tensile tests have a cylindrical shape with a gauge length of 10 mm and a gauge diameter of 5 mm. Both kinds of test samples are shown in Fig. 1. Tests were conducted at a strain rate of 10^{-3} s^{-1} at room temperature in a deformation dilatometer DIL 805A/D (TA Instruments) modified for the synchrotron radiation. Diffraction patterns were recorded using an exposure time of 0.5 s by a Perkin-Elmer XRD 1622 flat-panel detector with an array of 2048×2048 pixels and an effective pixel size of $200 \times 200 \mu\text{m}$. The beam energy was 100 keV, corresponding to a wavelength of 0.0124 nm. LaB₆ was used to

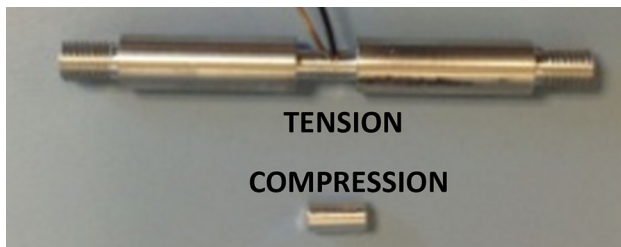


Fig. 1. Tensile and compressive samples used in the in situ diffraction experiments.

calibrate the acquired diffraction spectra. The detector-to-sample distance was set to 1637 mm. Debye-Scherrer rings gave the complete information from the extrusion to radial directions.

Conventional line profiles were obtained by azimuthal integration of the Debye-Scherrer rings, as shown Fig. 2. The synchrotron radiation beam was positioned at the center of the sample, with the gauge volume defined approximately by the beam section ($1 \times 1 \text{ mm}$) and the cylinder diameter. The elastic strain for each orientation can be calculated by the shift in the position of the diffraction peak, as:

$$\varepsilon_{hkl} = \frac{d_{hkl} - d_{0,hkl}}{d_{0,hkl}} \quad (1)$$

where d_{hkl} and $d_{0,hkl}$ are the planar spacing of the hkl plane in the stressed and stress-free crystals. The lattice spacing and the diffraction angle θ are related through Bragg's law.

RESULTS AND DISCUSSION

Microstructure

The micrographs in Fig. 3a-c show the microstructure of the three alloys in the as-cast state.

A dendritic microstructure consisting of magnesium dendrites (dark phase) and the LPSO phase (bright phase) located at the inter-dendritic space can be seen. The volume fraction of the LPSO phase, measured in a previous paper, increases with the increase in the yttrium and zinc content, with values of 7, 19, and 32%, respectively.¹⁷

After the extrusion at 350°C, the LPSO phase deforms plastically, developing an irregular fiber shape oriented parallel to the extrusion direction, while the Mg matrix is partially recrystallized. Fine equiaxed DRXed α -Mg grains surround coarse deformed α -Mg grains, which are elongated along the extrusion direction (non-DRXed) as seen in Fig. 3d-f. A detail at higher magnification of the microstructural constituents, such as DRXed and

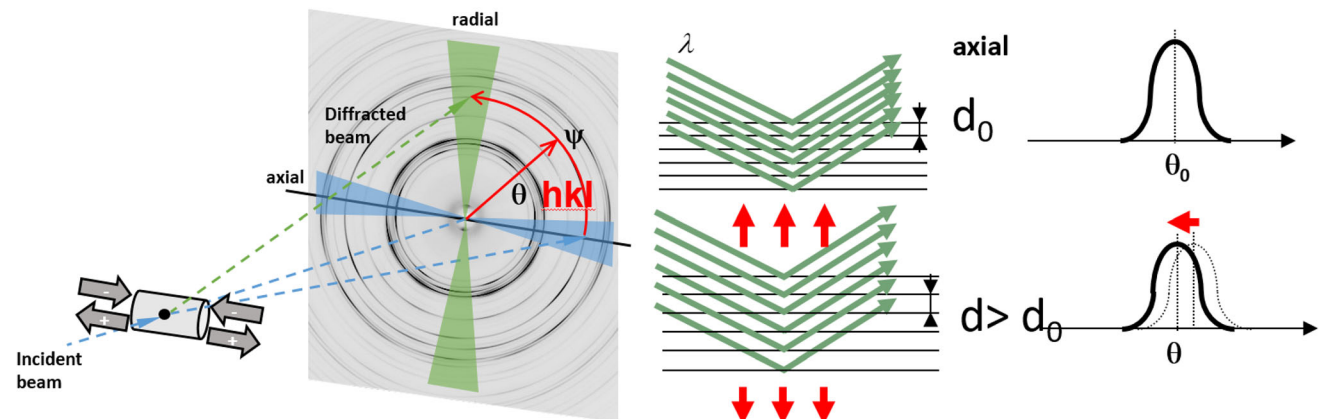


Fig. 2. Schematic of the in situ diffraction system and the diffraction peak due to lattice contraction and extension effect.

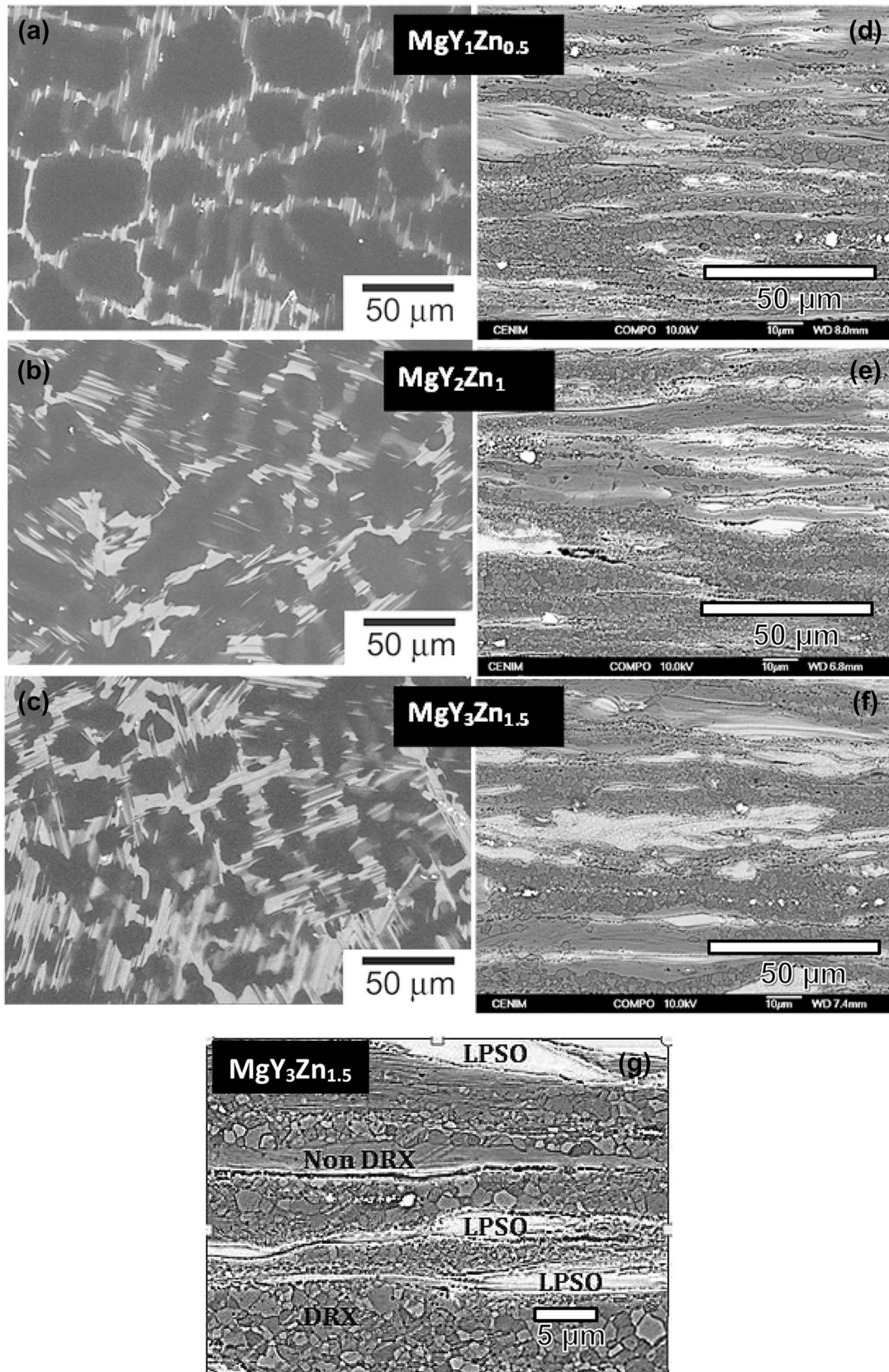


Fig. 3. Microstructure of the three Mg alloys in the as-cast state (a, b, c) and after extrusion at $\epsilon_7 = 2.3$ (d, e, f), and a detail at higher magnifications showing the microstructural constituents (g).

non DRXed α -Mg grains and elongated particles of the LPSO phase, is presented in Fig. 3g.

The volume fraction of DRXed α -Mg grains depends on both the extrusion ratio and the composition of the alloy. Thus, the volume fraction values of the DRXed and non-DRXed α -Mg grains for the three alloys extruded at the three extrusion ratios are presented in Table I. In general, except in the case of the $\text{MgY}_3\text{Zn}_{1.5}$ alloy extruded at $\varepsilon_T = 1.4$, it can be concluded that, for each alloy, the volume fraction of fine-grained DRXed areas increases with the extrusion strain, and that the opposite occurs for coarse-grained non-DRXed regions. These values have been plotted as a function of the volume fraction of LPSO phase in Fig. 4. In addition, a dashed line representing the same volume fraction of both types of grains, but subtracting the volume fraction of the LPSO, is also plotted. From this graph, it can be seen that the volume fraction of fine-grained DRXed areas is in general higher when the volume fraction of the LPSO phase and the extrusion ratio are also higher, i.e., with an increase in the total deformation strain. The values for the alloys extruded at $\varepsilon_T = 2.3$ and 2.9, are similar, while they are lower for the alloys extruded at an extrusion strain of 1.4. The LPSO phase promotes the recrystallization process in Mg-Y-Zn alloys.²⁰ Therefore, if the volume fraction of the LPSO phase increases, the volume fraction of the DRXed areas also increases. In the same way, a higher extrusion ratio causes a greater degree of deformation in the material, which will promote a faster recrystallization than that extruded to a lower extrusion ratio.

Figure 5 shows the grain size distribution in DRXed areas as a function of the alloy composition (or volume fraction of the LPSO phase), and the extrusion strain. From Fig. 5a it can be deduced

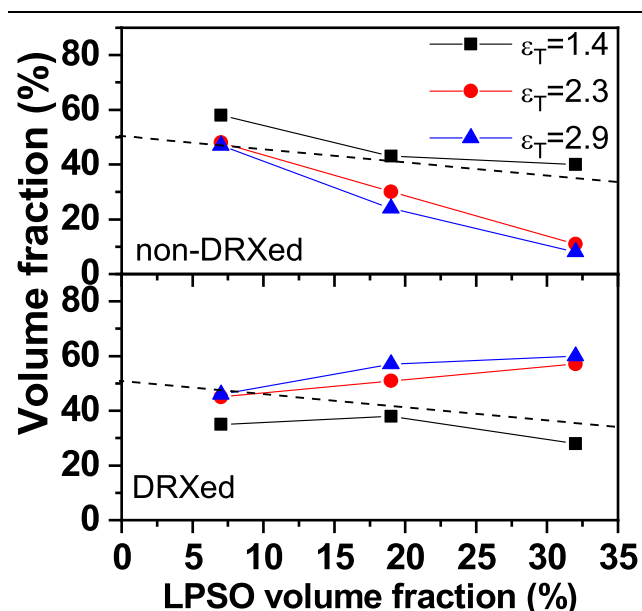


Fig. 4. Volume fractions of DRXed and non-DRXed α -Mg grains areas as a function of the extrusion strain for the three alloys.

that the grain size is similar for the three extruded alloys for the same extrusion strain. For a given composition, however, the increase in the extrusion strain slightly refines the grain (Fig. 5b), but always in a range close to $1 \mu\text{m}$.

The effects of the extrusion strain and the volume fraction of the LPSO phase on the texture of the alloys were also studied using x-ray diffraction with Cu-K α radiation. Figure 6 shows, as an example, the $\{10\bar{1}0\}$ and $\{0002\}$ pole figures for the extruded $\text{MgY}_1\text{Zn}_{0.5}$ at the lowest extrusion ratio. These figures indicate that the Mg matrix has a strong fiber texture with the basal plane parallel to the extrusion direction. The maximum of the intensity of the $\{10\bar{1}0\}$ pole figure at $\theta = 0^\circ$ varies with the alloy composition and the extrusion ratio, as shown in Fig. 6c. This graph demonstrates that the texture is stronger for the alloy with the lowest volume fraction of the LPSO phase and higher extrusion strains, as expected, although the highest intensity was measured for an extrusion strain of 2.3.

The texture is directly related to the non-DRXed α -Mg grains. Figure 7 shows the intensity of the $\{10\bar{1}0\}$ pole figure at $\theta = 0^\circ$ as a function of the volume fraction of the DRXed and non-DRXed α -Mg grains. It can be observed that the intensity of the crystallographic texture decays in the same way as the volume fraction of the non-DRXed α -Mg grains decreases.

Mechanical Properties

The yield stress values obtained from the tensile and compressive tests during in situ experiments of the three extruded alloys at the three different strains are presented in Table II and plotted in Fig. 8a.

The yield stress increases as the volume fraction of the LPSO phase becomes higher, regardless of the stress sign, tension, or compression. A similar tendency is found with an increase in the extrusion strain. However, the evolution of the tension–compression asymmetry depends on both parameters, as deduced from Fig. 8a. Thus, the alloy with the lowest volume fraction of the LPSO phase ($\text{MgY}_1\text{Zn}_{0.5}$) always presents a yield stress higher in tension than in compression, in agreement with the asymmetric behavior usually described in extruded Mg alloys, but the differences become smaller as the extrusion strain becomes higher (see Table II).

However, the $\text{MgY}_3\text{Zn}_{1.5}$ alloy, with the highest volume fraction of the LPSO phase, always exhibits abnormal yield stress asymmetry, since the value in compression is always higher than in tension, although both values are very close, independently of the extrusion strain. In the case of the MgY_2Zn_1 alloy, however, the tension–compression asymmetry depends on the processing strain, as observed in Fig. 8b. The alloy shows the usual behavior for ε_T

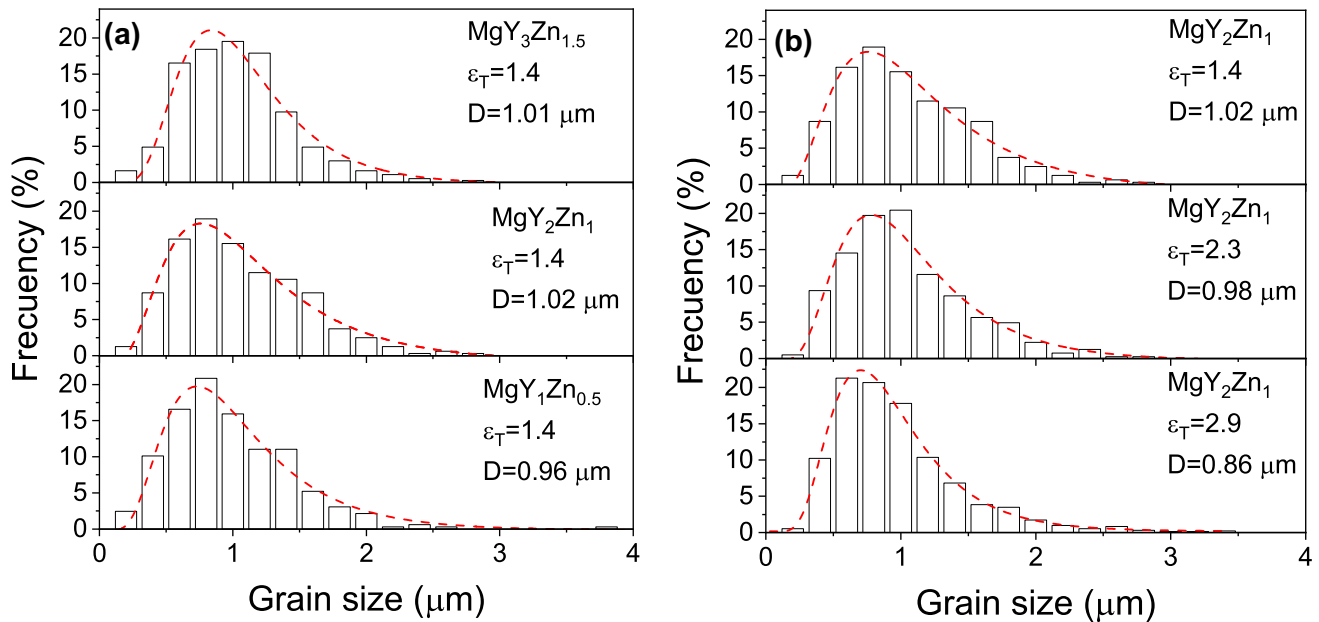


Fig. 5. Grain size distribution in DRXed areas as a function of the alloy composition, i.e., volume fractions of the LPSO phase, and extrusion strain: (a) effect of the volume fraction of LPSO phase when the extrusion strain remains constant, (b) effect of extrusion strain for a constant volume fraction of the LPSO phase.

= 1.4 and an anomalous behavior for $\varepsilon_T = 2.9$, as commented on the Introduction.

In Situ Diffraction Experiments

Figure 9 shows axial and radial diffraction patterns in the $\text{MgY}_3\text{Zn}_{1.5}$ alloy for the extrusion strain $\varepsilon_T = 2.3$. Similar patterns were obtained for the $\text{MgY}_1\text{Zn}_{0.5}$, MgY_2Zn_1 , and $\text{MgY}_3\text{Zn}_{1.5}$ alloys extruded at the different reduction ratios. The figure shows the intense fiber texture with the basal plane parallel to the extrusion direction of the magnesium matrix, in agreement with that shown in Fig. 6.

Figures 10 and 11 show the experimental results obtained from in situ experiments in two cases where the tension–compression asymmetry of the yield stress exhibits a reverse behavior, as a function of the microstructure or processing parameters: the extruded MgY_2Zn_1 alloy for the three processing strains (Fig. 10) and the three alloys extruded at processing strain of 2.3 (Fig. 11).

For each pair of conditions, the alloy composition, i.e., the volume fraction of the LPSO phase and the extrusion ratio, the evolution of the elastic strains of the diffraction peaks $\{10\bar{1}0\}$, $\{0002\}$, $\{10\bar{1}1\}$, and $\{11\bar{2}0\}$ of the Mg phase in the axial direction, as a function of the applied stress during the tensile and compressive experiments, are shown. Tensile and compressive curves, obtained during the in situ experiments, are also plotted to correlate the stages of the deformation (elastic and plastic regimes) with the evolution of the elastic strains. Moreover, the integrated intensity of the diffracted peaks in the axial direction for the $\{10\bar{1}0\}$ and $\{0002\}$ diffraction

peaks are also plotted as a function of the applied stress. The evolution of the intensity for these two diffracted peaks gives valuable information about the activation of the tensile $\{01\bar{1}2\}\langle 0\bar{1}11\rangle$ twinning system. The rotation of 86° of the basal plane with respect to its original orientation results in a change in the intensity of both diffraction peaks, i.e., the intensity of the $\{0002\}$ diffraction peak increases at the expense of the $\{10\bar{1}0\}$ diffraction peak.^{21,22}

The information about the elastic–plastic behavior of the non-DRXed and DRX α -Mg grains can be studied separately following the $\{10\bar{1}0\}$ and $\{10\bar{1}1\}$ diffraction peaks.¹⁰ On the other hand, due to the strong fiber texture of the Mg matrix in which the basal planes are parallel to the extrusion direction, the intensity of the $\{0002\}$ diffraction peak in the axial direction is extremely low (see Fig. 9a). Therefore, the evolution of the $\{0002\}$ diffraction peak will provide the elastic–plastic behavior of tensile twins.

Effect of the Extrusion Strain

The shape of the curves showing the evolution of the elastic strains for the MgY_2Zn_1 alloy during tensile or compressive tests is similar, independently of the extrusion ratio. In the elastic regime, in tension and compression, the evolution of the elastic strains is equal for all the diffraction peaks, due to the near-elastic isotropy behavior of Mg.²³ In tension, this linear behavior is broken at an applied stress below the macroscopic yield stress. At this point, the elastic strains of grains with $\{10\bar{1}1\}$ planes perpendicular to the tensile axis decrease continuously with respect to the linear elastic slope. In an opposite way, the elastic strains of grains with

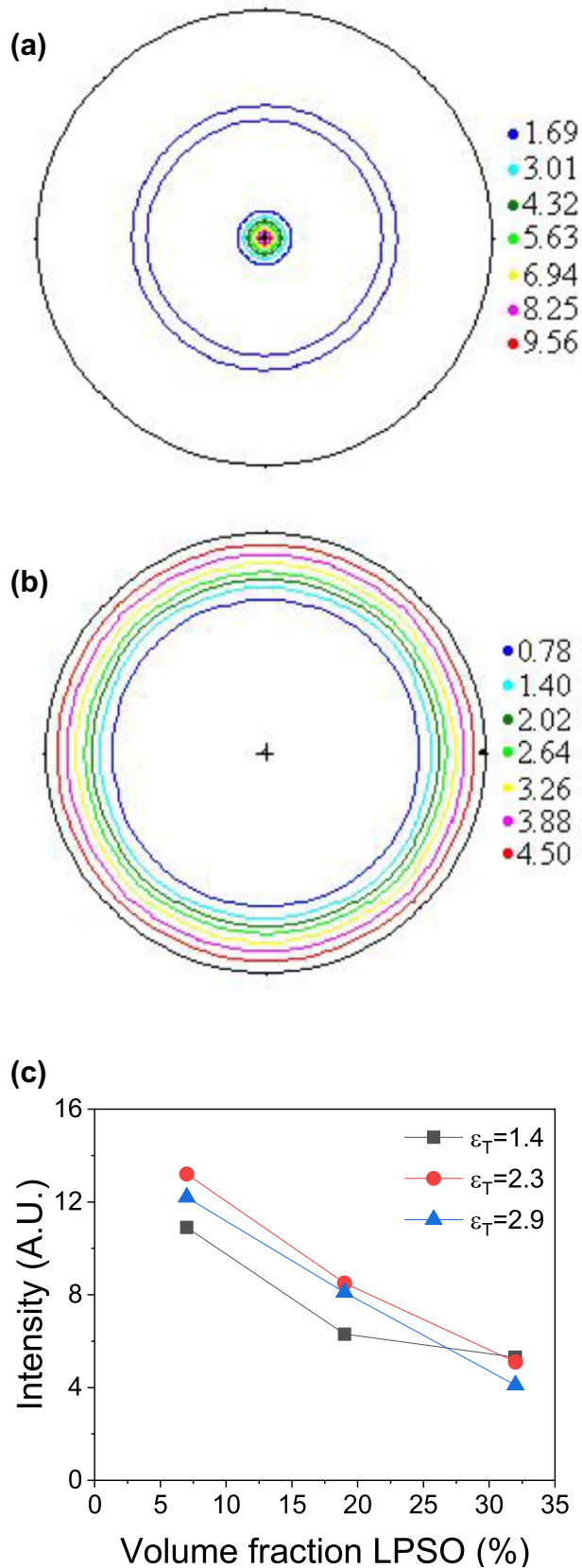


Fig. 6. (a and b) $\{10\bar{1}0\}$ and $\{0002\}$ pole figures, respectively, for the extruded $\text{MgY}_1\text{Zn}_{0.5}$ alloy at the processing strain of 1.4. (c) Maximum intensity plot of the $\{10\bar{1}0\}$ pole figure at $\theta = 0^\circ$ for the three alloys extruded at the three extrusion strains (1.4, 2.3, and 2.9).

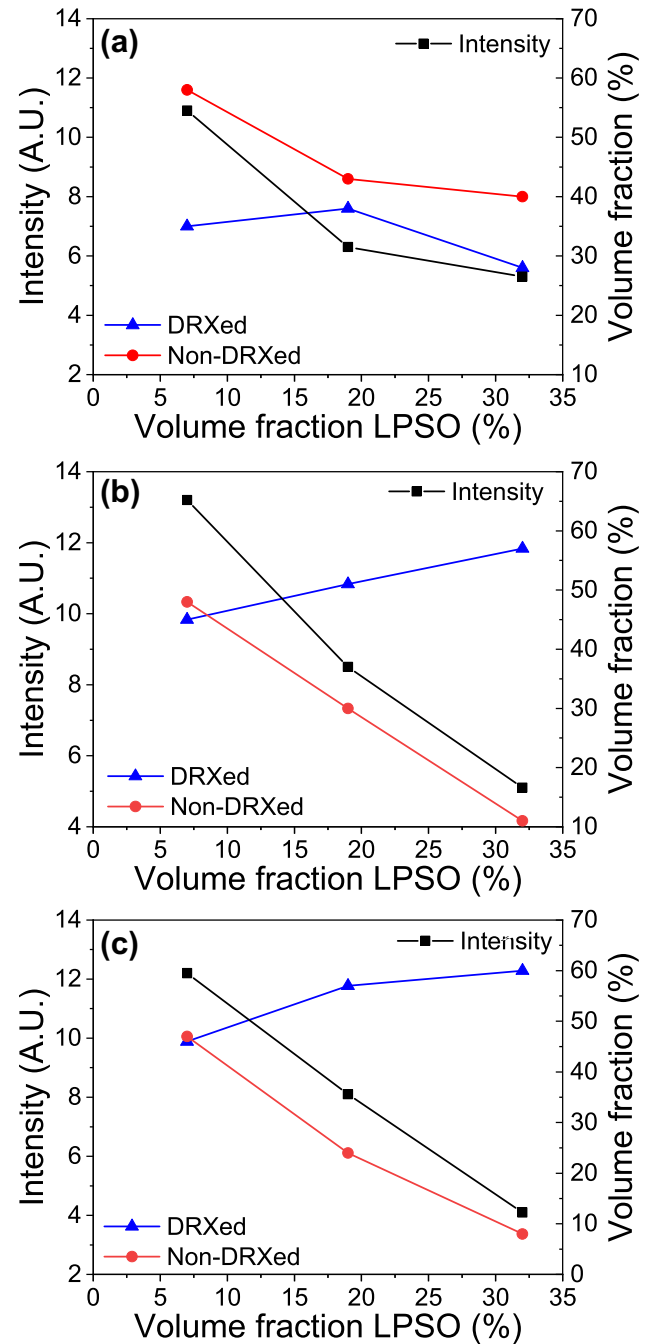


Fig. 7. Evolution of the volume fractions of DRXed and non-DRXed α -Mg grains and the maximum intensity in the $\{10\bar{1}0\}$ pole figure at $\theta = 0^\circ$, as a function of the volume fraction of the LPSO phase for the different processing strains: (a) 1.4, (b) 2.3, and (c) 2.9.

$\{10\bar{1}0\}$ and $\{11\bar{2}0\}$ planes perpendicular to the tensile axis increase with respect to the linear elastic slope. When the elastic strains in a phase or in a family of grains are greater than the strain defined by the elastic behavior, these “hard” phase or family of grains are bearing a load higher than the applied stress. The orientation of these grains inhibits the activation of the basal slip system. This additional stress is transferred from the $\{10\bar{1}1\}$ “soft” grains, which are favorably oriented for the

Table II. Yield stress values, in MPa, obtained from in situ tensile and compression experiments for the three extruded alloys

LPSO, V_v %	$\epsilon_T = 1.4$		$\epsilon_T = 2.3$		$\epsilon_T = 2.9$	
	Tension	Compression	Tension	Compression	Tension	Compression
7	319	252	324	278	322	282
19	321	301	353	353	333	381
32	346	352	360	383	374	387

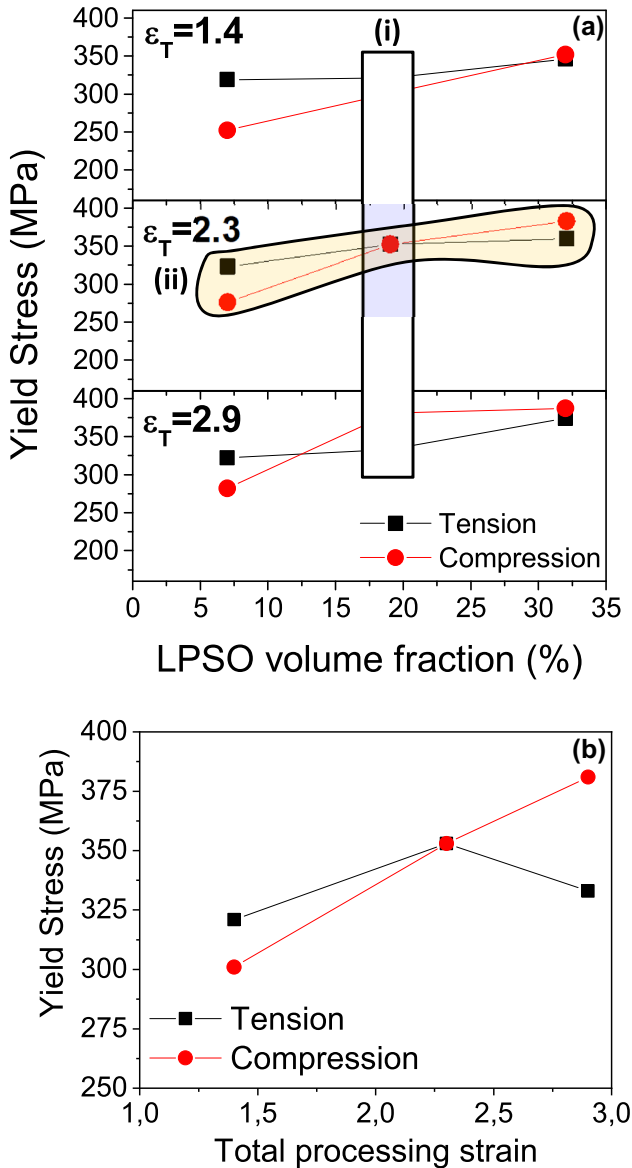


Fig. 8. Yield stress values from tension and compression tests: (a) variation of yield stress value as a function of the volume fraction of the LPSO phase for the three processing strains; the colored regions refer to the two cases described in detail in the Results and Discussion section; (b) variation of tensile and compressive yield stress values in the MgY_2Zn_1 alloy as a function of the processing strain.

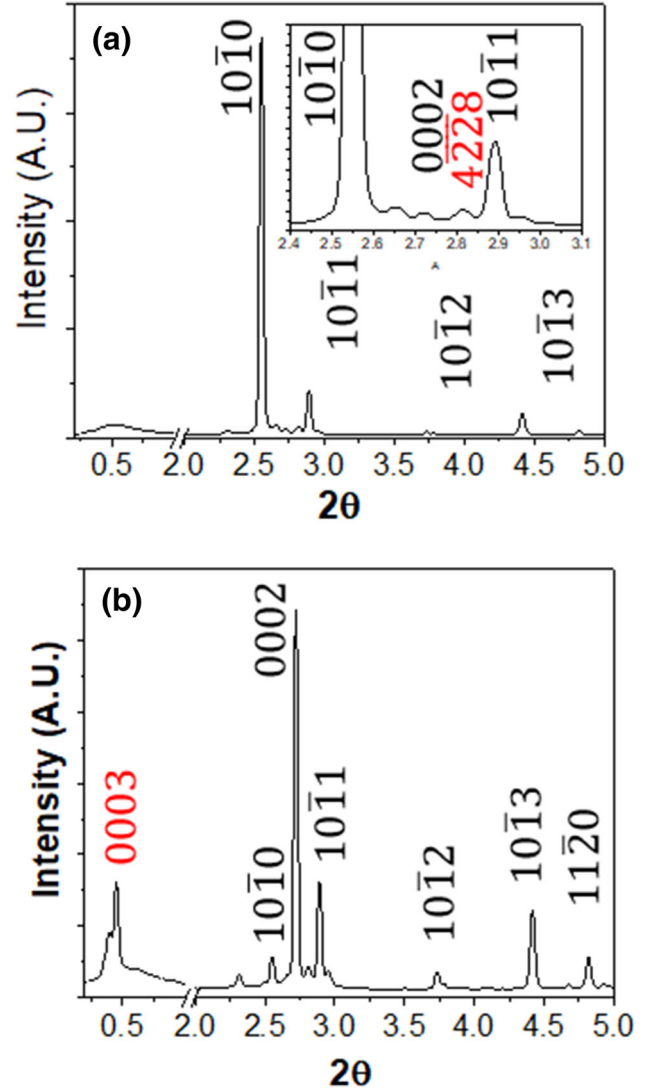


Fig. 9. $\text{MgY}_3\text{Zn}_{1.5}$ alloy: (a) axial and (b) radial diffraction patterns for the extrusion strain $\epsilon_T = 2.3$.

activation of the basal slip system.²³ As the volume fraction of the non-DRXed grains increases, the reinforcing effect of these hard grains will increase. It is important to point out that the relaxation of grains with $\{10\bar{1}1\}$ planes perpendicular to the stress axis ends/stops at a strain close to 0.0004.

A similar behavior is found during the compression tests, although with small differences. In the

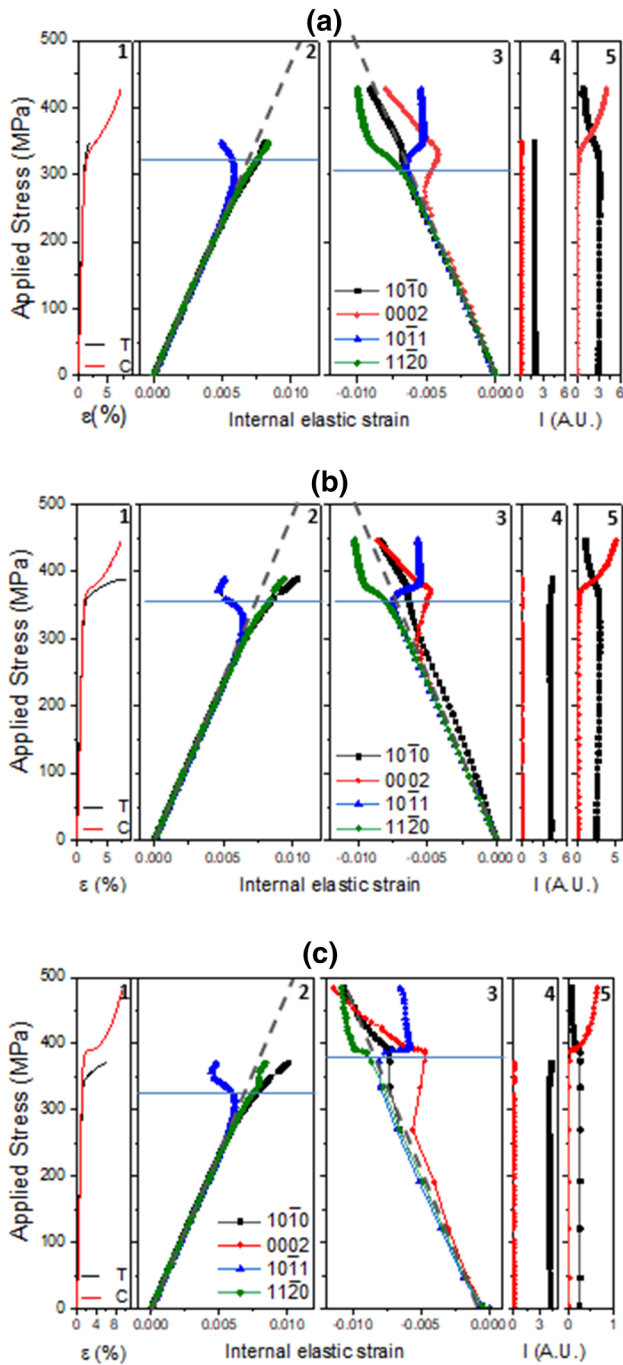


Fig. 10. Tensile and compressive behavior during in situ experiments of the MgY_2Zn_1 alloy extruded at different strains: (a) $\varepsilon_T = 1.4$, (b) $\varepsilon_T = 2.3$, and (c) $\varepsilon_T = 2.9$. From left to right: 1 macroscopic stress-strain curves, 2, 3 axial internal strains for the $\{10\bar{1}0\}$, $\{0002\}$, $\{10\bar{1}1\}$, and $\{11\bar{2}0\}$ diffraction peaks for the Mg phase as a function of the applied stress, in tension and compression, respectively, and 4, 5 evolution of the integrated intensity of the $\{10\bar{1}0\}$ and $\{0002\}$ diffraction peaks in the axial direction during tensile and compression tests.

elastic regime, the strains are equal for all the diffraction peaks, as found in the tension tests. However, the linear behavior is lost upon reaching the macroscopic yield point, which increases with

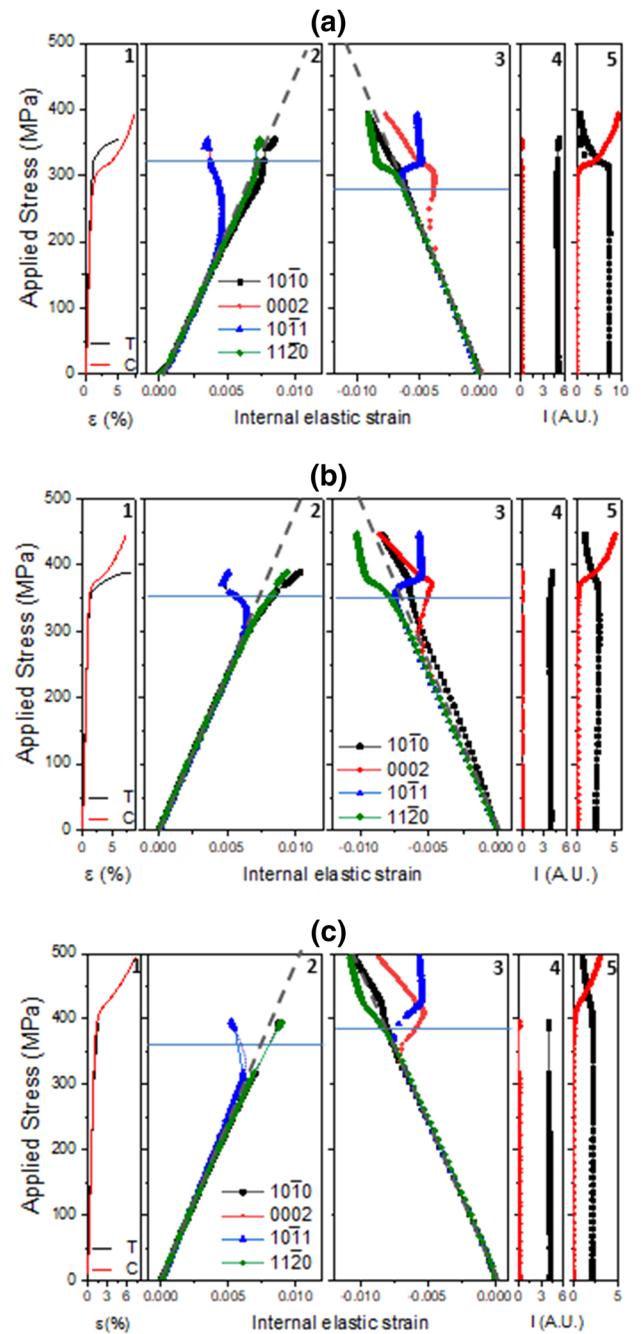


Fig. 11. Tensile and compressive behavior during in situ experiments of the (a) $\text{MgY}_1\text{Zn}_{0.5}$, (b) MgY_2Zn_1 , and (c) $\text{MgY}_3\text{Zn}_{1.5}$ alloys at $\varepsilon_T = 2.3$. From left to right: 1 macroscopic stress-strain curves, 2, 3 axial internal strains for the $\{10\bar{1}0\}$, $\{0002\}$, $\{10\bar{1}1\}$, and $\{11\bar{2}0\}$ diffraction peaks for the Mg phase as a function of the applied stress, in tension and compression, respectively, and 4, 5 evolution of the integrated intensity of the $\{10\bar{1}0\}$ and $\{0002\}$ diffraction peaks in the axial direction of tensile and compression tests.

the processing strain. At the yield stress, the elastic strains of grains with $\{10\bar{1}1\}$ planes perpendicular to the compression axis decrease continuously with respect to the linear elastic slope. In contrast, the elastic strains of grains with $\{11\bar{2}0\}$ planes perpendicular to the compressive axis increase with respect to the linear elastic slope. Unlike the tensile

tests, the elastic deformations of grains with $\{10\bar{1}0\}$ planes perpendicular to the compression axis have the same linear elastic slope as in the elastic regime. In the compression test, only grains with $\{11\bar{2}0\}$ planes perpendicular to the compression axis behave as “hard” grains. Under compression, grains oriented with the $\{10\bar{1}0\}$ perpendicular to the compressive axis yield due to the activation of tensile twinning. The increase in the intensity of the $\{0002\}$ diffraction peak confirms this assumption. Moreover, it is possible to evaluate the evolution of the elastic strain of this peak, due to the increase in the volume fraction of twins. The evolution of the elastic strain follows a linear behavior, as in the case of the other diffraction peaks, up to an applied stress around 275 MPa, similar for all the extrusion ratios but below the macroscopic yield stress. Then, the elastic strain decreases slightly in absolute values up to the applied stress when the intensity of the $\{0002\}$ begins to increase due to twin growth. Above this stress, the elastic strain decreases rapidly again. Between these two stress limits (stress corresponding to the limit of elastic linearity and beginning of the increase in $\{0002\}$ intensity), the nucleation and propagation of twins has been reported.²⁴

Effect of the Alloy Composition (Volume Fraction of LPSO Phase)

The evolution of the elastic strains for the three alloys extruded at an extrusion ratio of $\varepsilon_T = 2.3$ also shows a similar shape (Fig. 11) to the case described above. In the elastic regime, the evolution of the elastic strains is also equal for all the diffraction peaks. The behavior is linear at a stress below the macroscopic yield stress, although this stress increases with the volume fraction of the LPSO phase. The elastic strains of grains with $\{10\bar{1}1\}$ planes perpendicular to the tensile axis decrease continuously with respect to the linear elastic slope, while the elastic strains of grains with $\{10\bar{1}0\}$ and $\{11\bar{2}0\}$ planes perpendicular to the tensile axis increase with respect to the linear elastic slope. However, the reinforcing effect of hard grains increases as the volume fraction of the LPSO phase decreases and the volume fraction of non-recrystallized grains increases.

In the compression tests, the behavior of elastic strains of grains oriented with the $\{10\bar{1}0\}$, $\{10\bar{1}1\}$, and $\{11\bar{2}0\}$ planes perpendicular to the tensile axis is similar to that due to the effect of the extrusion rate. Deviation of elastic linearity by the internal strains also takes place at the macroscopic yield stress. This stress limit increases with the increase in the volume fraction of the LPSO phase and the decrease in the volume fraction of the non-DRXed grains. The stress for the activation of tensile twinning also increases with the increase in the volume fraction of the LPSO, and with the decrease

in the volume fraction of the non-DRXed grains. It must be remembered that the LPSO phase has a higher Young’s modulus and yield stress than those of the Mg matrix.²⁵ In addition, it exhibits a tension–compression asymmetry inverse to that of Mg, since its yield stress in compression is higher than in tension.²⁶

Therefore, all these microstructural parameters control the mechanical strength of Mg alloys containing LPSO phases, in such a way that these alloys can be considered as a composite, as previously discussed in detail.^{17,27} Accordingly, the yield stress, $\sigma_{0.2}$, can be roughly estimated using the rule of mixtures with the following expression:

$$\begin{aligned} \sigma_{0.2} = & f_{\text{LPSO}}\sigma_{\text{LPSO}} + f_{\text{DRXed}}\left(\sigma_0 + \sigma_{\text{HP}} + \sigma'_T\right)\sigma_{\text{DRXed}} \\ & + f_{\text{Non-DRXed}}\left(\sigma_0 + \sigma_{\text{HP}} + \sigma_T\right)\sigma_{\text{Non-DRXed}} \end{aligned} \quad (2)$$

where f_{LPSO} is the volume fraction of the LPSO phase, f_{DRXed} is the volume fraction of α -Mg areas with DRXed grains, $f_{\text{Non-DRXed}}$ is the volume fraction of coarse-grained non-DRXed regions, and σ_{LPSO} is the yield stress of the LPSO phase which depends on the deformation mode (tension or compression). For both kinds of α -Mg grains areas, DRXed and non-DRXed, two contributions have been taken into account: the grain size given by the Hall–Petch equation and the capacity to deform given by their crystal orientation or texture. σ'_T is negligible for DRXed grains due to random orientations that easily activate the basal slip system. σ_{HP} in non-DRXed grains also has a minor influence because of their coarse grain size, especially in the extrusion direction (several hundred times more than the size of DRXed grains). Therefore, Eq. 2 can be simplified into:

$$\begin{aligned} \sigma_{0.2} = & f_{\text{LPSO}}\sigma_{\text{LPSO}} + f_{\text{DRXed}}\left(\sigma_0 + \sigma_{\text{HP}}\right)\sigma_{\text{DRXed}} \\ & + f_{\text{Non-DRXed}}\left(\sigma_0 + \sigma_T\right)\sigma_{\text{Non-DRXed}} \end{aligned} \quad (3)$$

The contribution of the LPSO phase was determined from reference.¹⁷ Values of σ_0 and σ_{HP} were achieved from,²⁸ using $\sigma_0 = 49$ MPa and $k_{\text{HP}} = 188$ MPa $\mu\text{m}^{-1/2}$. Using the average grain size of DRXed grains, D_{DRXed} , obtained from Fig. 5, together with the recrystallized volume fractions areas, f_{DRXed} , the contributions to the yield stress from the fine-grained DRXed α -Mg grains can be calculated. Comparison of the experimental yield stress with the strengthening contributions of the LPSO phase and the DRXed grains finally allows the determination of the texture contribution due to non-DRXed α -Mg grains. Figure 12 shows the contributions to the yield stress of the LPSO phase and the non-DRXed and DRXed areas of the Mg matrix as a function of the volume fraction of the LPSO phase for the three extrusion strains. In all cases, the contribution of the LPSO phase is greater in compression than in tension, and differences grow

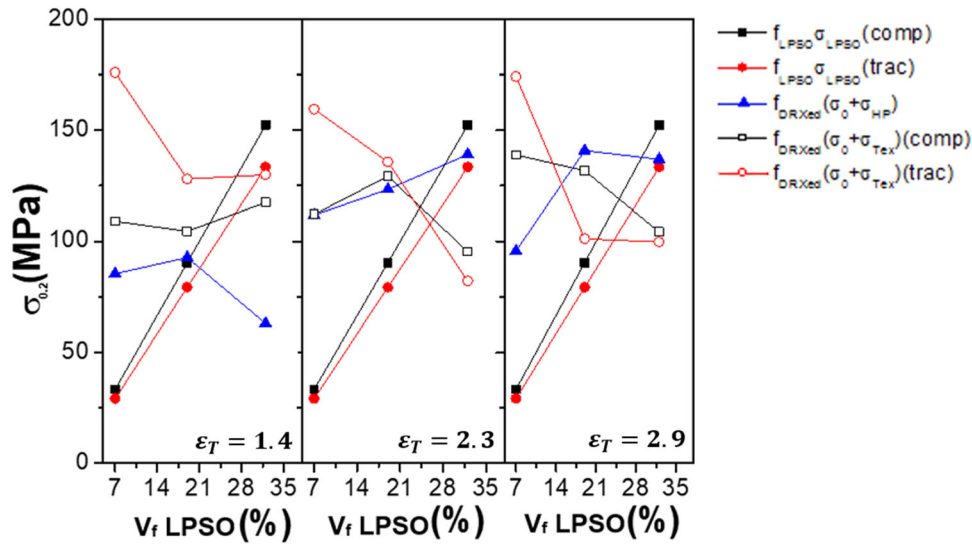


Fig. 12. The strengthening contributions, in both tension and compression, due to the different microstructural parameters for the three extruded alloys.

with the volume fraction of the LPSO phase. The contribution of the DRXed grains, according to the Hall–Petch equation, is the same for tension and compression. The refinement of the DRXed grains is the main contribution for the increase in the mechanical strength of these alloys. The increase in the extrusion strain continuously increases this contribution, especially for the alloy with the higher volume fraction of the LPSO phase, since it promotes the increase in the DRXed Mg areas.

The contribution of coarse non-DRXed α -Mg grains to the mechanical strength of these alloys, due to their crystallographic texture, depends on the deformation mode. These grains exhibit an elastic behavior during tensile tests, but they yield by the activation of tensile twinning during compression tests. In situ experiments confirmed such behavior (Figs. 10 and 11). Therefore, this contribution is completely different, depending on both kinds of mechanical tests. At processing strain of $\epsilon_T = 1.4$, the strengthening effect of the coarse grains in tension is higher (around 100 MPa) than in compression. On the other hand, at the processing strain of $\epsilon_T = 2.9$, the strengthening contribution in both tension and compression is similar.

Also, the deformation of these alloys is the sum of the separate deformation of each kind of α -Mg grains: recrystallized and non-recrystallized. DRXed grains deform by the activation of the basal slip system, independently of the deformation mode and the volume fraction of the LPSO phase. However, the elastic–plastic behavior of coarse non-DRXed grains depends on the deformation mode. On the one hand, under tension, non-DRXed grains deform almost elastically, and bear an additional load transferred by the DRXed grains. In order to accommodate the macroscopic strain of the DRXed grains, a non-basal slip system has been reported.²⁹ On the other hand, under compression, these grains

deform by the activation of tensile twinning. Therefore, when the volume fraction of highly textured non-DRXed grains is higher than the recrystallized areas, the alloy is stronger in tension than in compression (normal tension–compression asymmetry). However, when the volume fraction of the DRXed grains is higher than the non-recrystallized areas, the macroscopic strain is controlled by basal slip in the DRXed grains, and the alloy is stronger in compression than in tension because the LPSO phase controls this behavior.

CONCLUSION

The mechanical response in tension and compression, as well as the sign of tension–compression asymmetry, has been studied in Mg- Y_{2x} - Zn_x alloys as a function of the extrusion strain and volume fraction of the LPSO phase. Synchrotron diffraction experiments have been carried out during in situ mechanical tests to understand the deformation mode of the different constituents of the microstructure. The following conclusions can be drawn:

1. The microstructure of as-cast alloys consists of magnesium dendrites and the LPSO phase located in the inter-dendritic space. The volume fraction of the LPSO phase increases as the yttrium and zinc contents increase.
2. After extrusion at 350°C, the LPSO phase elongates along the extrusion direction and the magnesium matrix is partially recrystallized, showing areas of DRXed and non-DRXed grains.
3. A complete variety of microstructures can be obtained for the alloys containing different volume fractions of the LPSO phase by varying the extrusion strain.
4. The volume fraction of the DRXed grains grows with the increase in the volume fraction of the LPSO phase and the processing strain.

- Through in situ diffraction experiments, it has been possible to learn the individual elastic–plastic behavior of non-DRXed and DRXed α -Mg grains, their contribution to the macroscopic deformation, and the tension–compression asymmetry in these alloys.
- The tension–compression asymmetry in Mg-LPSO alloys with a low volume fraction of the LPSO phase is similar to that of classical extruded magnesium alloys when the volume fraction of non-DRXed highly oriented grains is much larger than that of DRXed grains. Under tension, non-DRXed grains favor the increase of the yield stress with respect to compression, since they behave as an elastic reinforcement. Under compression, they are easily deformed by twinning.
- In those alloys with a high volume fraction of the LPSO phase or processed at a high extrusion ratio, the tension–compression asymmetry is inverted, since DRXed grains control the onset of plasticity by activating basal slip.

ACKNOWLEDGEMENTS

We would like to acknowledge the financial support of the Spanish Ministry of Economy and Competitiveness under project number MAT2016-78850-R and the Czech Science Foundation under the contract 16-12075S. We also want to acknowledge the expert support of Miguel Acedo and Edurne Laurin for assistance with extrusion processing and metallographic preparation, respectively. The Deutsches Elektronen-Synchrotron DESY is acknowledged for the provision of beamtime at the P07 beamline of the Petra III synchrotron facility in the framework of proposal I-20140200 EC.

FUNDING

Open Access funding provided thanks to the CRUE-CSIC agreement with Springer Nature.

CONFLICT OF INTEREST

On behalf of all authors, the corresponding author states that there is no conflict of interest.

OPEN ACCESS

This article is licensed under a Creative Commons Attribution 4.0 International License, which permits use, sharing, adaptation, distribution and reproduction in any medium or format, as long as you give appropriate credit to the original author(s) and the source, provide a link to the Creative Commons licence, and indicate if changes were made. The images or other third party material in this article are included in the article's Creative Commons licence, unless indicated otherwise in a credit line to the material. If material is not included in the article's Creative Commons licence and your intended use is not permitted by statutory

regulation or exceeds the permitted use, you will need to obtain permission directly from the copyright holder. To view a copy of this licence, visit <http://creativecommons.org/licenses/by/4.0/>.

REFERENCES

- A. Inoue, Y. Kawamura, M. Matsushita, K. Hayashi, and J. Koike, *J. Mater. Res.* 21, 1894. <https://doi.org/10.1557/JMR.2001.0260> (2005).
- Y. Kawamura, and M. Yamasaki, *Mater. Trans.* 48, 2986. <https://doi.org/10.2320/matertrans.MER2007142> (2007).
- D. Egusa, and E. Abe, *Acta Mater.* 60, 166. <https://doi.org/10.1016/j.actamat.2011.09.030> (2012).
- K. Kishida, K. Nagai, A. Matsumoto, A. Yasuhara, and H. Inui, *Acta Mater.* 99, 228. <https://doi.org/10.1016/j.actamat.2015.08.004> (2015).
- G. Garcés, P. Pérez, S. González, and P. Adeva, *Int. J. Mater. Res.* 97, 404. <https://doi.org/10.3139/146.101231> (2006).
- M. Yamasaki, K. Hashimoto, K. Hagihara, and Y. Kawamura, *Acta Mater.* 59, 3646. <https://doi.org/10.1016/j.actamat.2011.02.038> (2011).
- G. Garces, P. Pérez, S. Cabeza, S. Kabra, W. Gan, and P. Adeva, *Metal. Mater. Trans. A* 48, 5332. <https://doi.org/10.1007/s11661-017-4284-6> (2017).
- K. Hagihara, N. Yokotani, and Y. Umakoshi, *Intermetallics* 18, 267. <https://doi.org/10.1016/j.intermet.2009.07.014> (2010).
- M. Arul Kumar, I.J. Beyerlein, and C.N. Tomé, *J. Alloy. Compd.* 695, 1488. <https://doi.org/10.1016/j.jallcom.2016.10.287> (2017).
- J. Schmidt, I.J. Beyerlein, M. Knezevic, and W. Reimers, *Metals* 11, 37. <https://doi.org/10.3390/met11030377> (2021).
- K. Frydrych, T. Libura, Z. Kowalewski, M. Maj, and K. Kowalczyk-Gajewska, *Mater. Sci. Eng. A* 813, 141152. <https://doi.org/10.1016/j.msea.2021.141152> (2021).
- X. Huang, Y. Xin, Y. Cao, G. Huang, and W. Li, *J. Mater. Sci. Technol.* 109, 30. <https://doi.org/10.1016/j.jmst.2021.07.051> (2022).
- J. Xu, B. Guan, Y. Xin, X. Wei, G. Huang, and C. Liu, *J. Mater. Sci. Technol.* 99, 251. <https://doi.org/10.1016/j.jmst.2021.04.076> (2021).
- S. Kleiner, and P.J. Uggowitzer, *Mat. Sci. Eng. A* 379, 258. <https://doi.org/10.1016/j.msea.2004.02.020> (2004).
- S.H. Park, J.H. Lee, B.G. Moon, and B.S. You, *J. Alloy. Compd.* 617, 277. <https://doi.org/10.1016/j.jallcom.2014.07.164> (2014).
- Y. Baia, B. Yea, J. Guoa, L. Wanga, X. Kongb, and W. Ding, *Mat. Charact.* 164, 110301. <https://doi.org/10.1016/j.matchar.2020.110301> (2020).
- G. Garces, P. Perez, S. Cabeza, H.K. Lin, S. Kim, W. Gan, and P. Adeva, *Mater. Sci. Eng. A* 647, 287. <https://doi.org/10.1016/j.msea.2015.09.003> (2015).
- G. Garces, D.G. Morris, M.A. Muñoz-Morris, P. Perez, D. Tolnai, C. Mendis, A. Stark, H.K. Lim, S. Kim, N. Shell, and P. Adeva, *Acta Mater.* 94, 78. <https://doi.org/10.1016/j.actamat.2015.04.048> (2015).
- G. Garcés, K. Máthis, J. Medina, K. Horváth, D. Drozdenko, E. Oñorbe, P. Dobroň, P. Pérez, M. Klaus, and P. Adeva, *Int. J. Plasty.* 106, 107. <https://doi.org/10.1016/j.ijplas.2018.03.004> (2018).
- E. Oñorbe, G. Garces, P. Pérez, and P. Adeva, *J. Mater. Sci.* 47, 1085. <https://doi.org/10.1007/s10853-011-5899-4> (2012).
- M.A. Gharghoury, G.C. Weatherly, J.D. Embury, and J. Root, *Phil. Mag. A* 79, 1671. <https://doi.org/10.1080/01418619908210386> (1999).
- B. Clausen, C.N. Tomé, D.W. Brown, and S.R. Agnew, *Acta Mater.* 56, 2456. <https://doi.org/10.1016/j.actamat.2008.01.057> (2008).
- S.R. Agnew, D.W. Brown, and C.N. Tome, *Acta Mater.* 54, 4841. <https://doi.org/10.1016/j.actamat.2006.06.020> (2006).
- G. Garces, K. Máthis, R. Barea, J. Medina, P. Pérez, A. Stark, N. Schell, and P. Adeva, *Mater. Sci. Eng. A* 768, 138452. <https://doi.org/10.1016/j.msea.2019.138452> (2019).

25. M. Tane, Y. Nagai, H. Kimizuka, K. Hagihara, and Y. Kawamura, *Acta Mater.* 61, 6338. <https://doi.org/10.1016/j.actamat.2013.06.041> (2013).
26. G. Garces, M.A. Muñoz-Morris, D.G. Morris, J.A. Jimenez, P. Perez, and P. Adeva, *Intermetallics* 55, 167. <https://doi.org/10.1016/j.intermet.2014.07.015> (2014).
27. G. Garces, M.A. Muñoz-Morris, D.G. Morris, P. Perez, and P. Adeva, *Mater. Sci. Eng. A* 614, 96. <https://doi.org/10.1016/j.msea.2014.07.012> (2014).
28. K. Hagihara, A. Kinoshita, Y. Sugino, M. Yamasaki, Y. Kawamura, H.Y. Yasuda, and Y. Umakoshi, *Acta Mater.* 58, 6282. <https://doi.org/10.1016/j.actamat.2010.07.050> (2010).
29. G. Garcés, A. Orozco-Caballero, J. Quinta da Fonseca, P. Pérez, J. Medina, A. Stark, N. Schell, and P. Adeva, *Mater. Sci. Eng. A.* 772, 138716. <https://doi.org/10.1016/j.msea.2019.138716> (2020).

Publisher's Note Springer Nature remains neutral with regard to jurisdictional claims in published maps and institutional affiliations.